Bull. Soc. R. Sci. Liège, 2024, **93**(3), 324–337 *Peer-reviewed conference paper*
doi:10.25518/0037-9565.12401

High-mass X-ray Binaries in Milky Way/Andromeda-like Galaxies

Felipe VIVANCO CÁDIZ[1,*], M. Celeste ARTALE[1], Nicola MASETTI[2,1], Gastón J. ESCOBAR[3,4] and Giuliano IORIO[3,4,5]

[1] Universidad Andres Bello, Facultad de Ciencias Exactas, Departamento de Ciencias Físicas, Instituto de Astrofísica, Av. Fernández Concha 700, Santiago, Chile
[2] Istituto Nazionale di Astrofisica, Osservatorio di Astrofisica e Scienza dello Spazio di Bologna, Via Gobetti 101, I–40129, Bologna, Italy
[3] Physics and Astronomy Department Galileo Galilei, University of Padova, Vicolo dell'Osservatorio 3, I–35122, Padova, Italy
[4] INFN – Padova, Via Marzolo 8, I–35131 Padova, Italy
[5] INAF – Padova, Vicolo dell'Osservatorio 5, I–35122 Padova, Italy
[*] Corresponding author: fvivanco@me.com

Paper presented at the 41st Liège International Astrophysical Colloquium on "The eventful life of massive star multiples," University of Liège (Belgium), 15–19 July 2024.

Abstract

High-Mass X-ray Binaries (HMXBs) are important for the study of the evolution of massive stars, the formation of compact objects such as black holes (BH) and neutron stars (NS), and the binary evolution processes that govern these systems. Moreover, HMXBs are crucial for understanding the accretion processes responsible for X-ray emission and are also potential progenitors of gravitational wave (GW) sources. In this study, we explore the population of HMXBs within simulated MW/M31-like galaxies by employing the IllustrisTNG50 hydrodynamical simulation in combination with the SEVN population synthesis code. We populate these galaxies with HMXBs by selecting stellar particles based on spatial location, metallicity, and age, accounting for the effects of varying metallicities and binary evolution processes. Our results indicate that the number and luminosity of HMXBs are significantly influenced by metallicity, confirming previous findings. Furthermore, we reproduce the expected slopes of the X-ray luminosity function (XLF), as well as the orbital parameters and masses of these systems, finding that the power-law slope α of the XLF is within the observed range and consistent with Galactic observational data.

Keywords: X-rays: binaries, Galaxies: stellar content, Galaxies: evolution

1. Introduction

High-Mass X-ray Binaries (HMXBs) are binary systems consisting of a compact object, either a black hole (BH) or a neutron star (NS), and a high-mass companion star with a mass

greater than $8\,M_{\odot}$. These systems emit X-rays due to the accretion of material from the companion star, which heats up as it falls onto the compact object. The material transfer can occur via stellar winds or Roche-lobe overflow (RLOF), producing X-ray luminosities ranging from 10^{35} to 10^{38} erg/s. HMXBs are generally found in regions of recent star formation (Grimm et al., 2003) and are expected to be more luminous in low-metallicity environments (Dray, 2006; Lehmer et al., 2021). Furthermore, the X-ray luminosity function (XLF) of these systems correlates with the star-formation rate (SFR) of their host galaxies (Mineo et al., 2012) and these objects tend to be more numerous in metal-poor galaxies than in metal-rich ones (see, e.g., Mapelli et al., 2009; Douna et al., 2015).

HMXBs are considered potential progenitors of binary compact object mergers and precursors of gravitational wave events (van den Heuvel, 2019). However, observational selection effects complicate the interpretation of this comparison, and their connection remains poorly established (see, e.g., Fishbach and Kalogera, 2022). In this scenario, population synthesis models serve as valuable tools for elucidating their connection. Furthermore, studying the observed Galactic HMXB population alongside results from population synthesis models can provide valuable insights into their formation and evolution.

In this work, we model the population of HMXBs in Milky Way- and M31-like galaxies. We investigate how metallicity affects the HMXB population generated by our model using a population synthesis code. This influence is particularly evident in characteristics like X-ray luminosity and the total number of systems. We then compare our results with the literature. After populating the galaxies with simulated HMXBs, we examine the properties of the latter, including the masses of the binaries, orbital parameters, and the slope of their X-ray luminosity function, and contrast these results with observational data from the Milky Way.

In Sect. 2, we present the methodology. We provide a description of the HMXBs model and galaxy catalogs. In Sect. 3, we present the results and compare them with the observational data. We summarize the main conclusions in Sect. 4.

2. Methodology

2.1. SEVN - Initial Conditions

We use the population synthesis code SEVN (Stellar EVolution *N*-body; Spera et al. 2015; Iorio et al. 2023), which employs stellar tracks computed with PARSEC (Bressan et al., 2012; Nguyen et al., 2022) to generate the catalogs of HMXBs. The parameters of our binary simulation are based on the fiducial model used in Iorio et al. (2023). However, we adopt the following modifications: i) we employ the delayed supernova model from Fryer et al. (2012); ii) we increase the accretion efficiency during RLOF, $f_{\rm MT}$, from 0.5 to 1; iii) we set the common envelope efficiency $\alpha_{\rm CE} = 0.5$, as this value provided the best match to observational data after conducting multiple tests aimed at simulating HMXB systems; iv) we apply the RLOF formalism by Hurley et al. (2002) but including the propeller effect to limit the accretion on NS following Campana et al. (2018) and implemented by Sgalletta et al. (2023) in SEVN; and v) we adopt a maximum mass for NS of $2.3\,M_{\odot}$ instead of $3.0\,M_{\odot}$ (Nathanail et al., 2021). Table 1 outlines the changes made in comparison to the fiducial model of Iorio et al. (2023).

Table 1: Parameter comparison between this work and the fiducial model in Iorio et al. (2023).

Parameters	Fiducial model	Model used in this work
Supernova model	Rapid[a]	Delayed[a]
Accretion efficiency during RLO	$f_{\rm MT} = 0.5$	$f_{\rm MT} = 1.0$
Common envelope efficiency	$\alpha_{\rm CE} = 0.5, 1, 3, 5$	$\alpha_{\rm CE} = 0.5$
RLOF formalism	Ref. b	Ref. b + propeller effect on NS
Maximum NS mass [$M_\odot$]	3.0	2.3

References: [a] Fryer et al. (2012); [b] Hurley et al. (2002)

We perform a set of runs using SEVN for 18 different metallicities Z ranging from 0.0002 to 0.04, each with a total of 10^7 binary systems. The primary mass is drawn from a Kroupa initial mass function (Kroupa, 2001), while the secondary mass, period and eccentricity distribution are obtained from Sana et al. (2012). The initial stellar spin for the stars is set to 0. The lower limit primary and secondary masses are set to $8\,M_\odot$, this to ensure that most of the population meets the selection criteria for HMXBs. This allows for a broader representation of the population across the simulated parameter space. We account for this incomplete sampling of the IMF, that goes from $M_{\rm min} = 8\,M_\odot$ to $M_{\rm max} = 150\,M_\odot$ with a correction factor, $f_{\rm corr}$.

2.1.1. Selection of HMXBs

We identify HMXBs from the simulation outputs using a criterion similar to that of Misra et al. (2023), and impose an X-ray luminosity threshold for the events.

The bolometric luminosity of each HMXB, $L_{\rm Bol}$, is calculated as

$$L_{\rm Bol} = \eta \dot{M} c^2 \quad \text{when} \quad \frac{\dot{M}}{\dot{M}_{\rm Edd}} \leq 1.0\,,$$

where $\dot{M}$ is the mass-accretion rate from the donor to the compact object via stellar winds and/or RLOF, $\dot{M}_{\rm Edd}$ is the Eddington mass-accretion rate, c is the speed of light, and η is the radiative efficiency. For NSs, the radiative efficiency is calculated as

$$\eta = \frac{G M_{\rm NS}}{R_{\rm NS} c^2}\,,$$

where G is the gravitational constant, and $M_{\rm NS}$ and $R_{\rm NS}$ are the mass and radius of the NS respectively. The radiative efficiency for BHs is calculated following Podsiadlowski et al. (2003) as:

$$\eta = 1 - \sqrt{1 - \left(\frac{M_{\rm BH}}{3\,M^0_{\rm BH}}\right)^2} \quad \text{for} \quad M_{\rm BH} < \sqrt{6}\,M^0_{\rm BH}\,,$$

where $M^0_{\rm BH}$ is the initial mass of the BH, and $M_{\rm BH}$ is the mass of the BH during the HMXB phase.

We turn the bolometric luminosity into X-ray luminosity within the 0.5 to 8 keV range of the *Chandra* band by applying the bolometric correction estimates provided by Fragos et al.

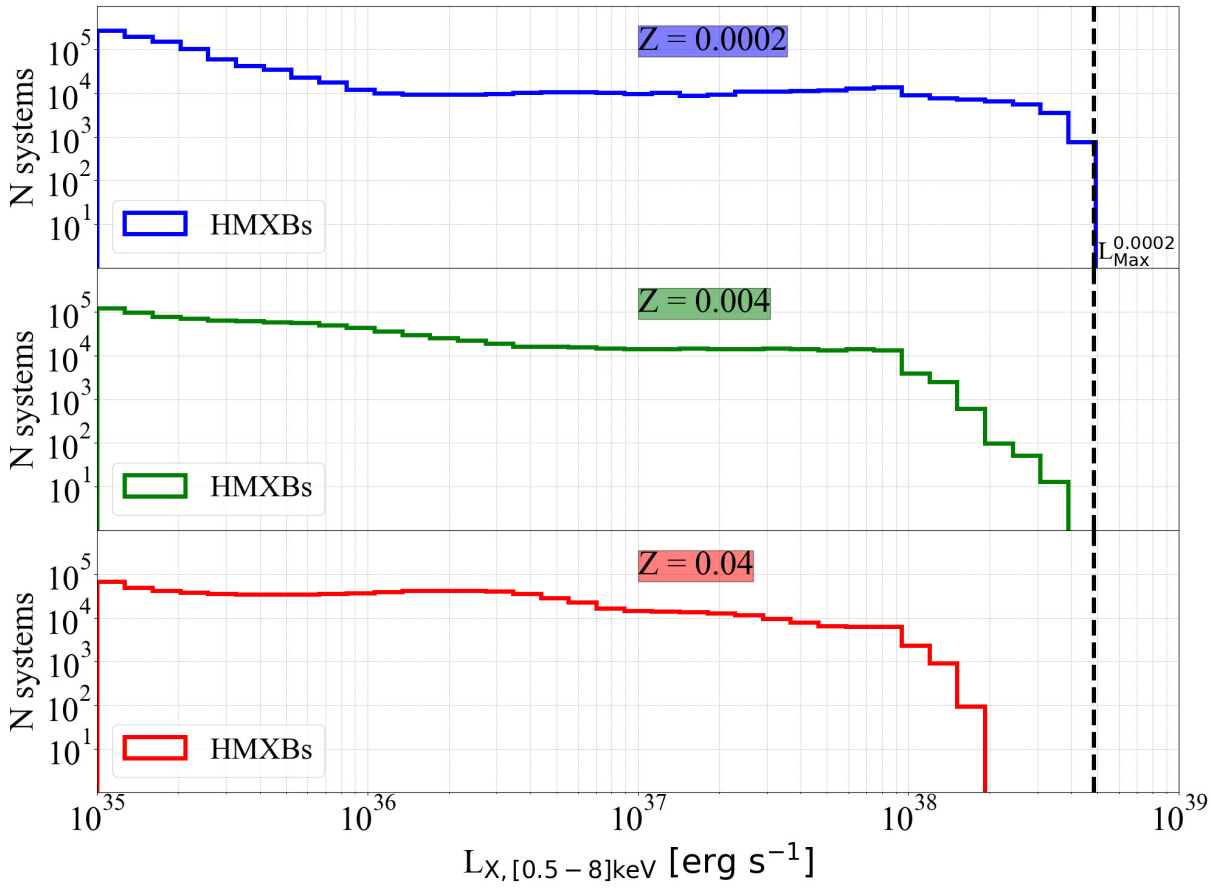

Figure 1: X-ray luminosity distribution of HMXBs of three different metallicities. The black dashed vertical line marks the maximum luminosity reached in the run with the lowest metallicity.

(2013) and Anastasopoulou et al. (2022):

$$L_{\mathrm{X},[0.5-8]\mathrm{keV}} = 0.5 \times L_{\mathrm{Bol}}\,.$$

Figure 1 shows X-ray luminosity distributions for HMXB systems at three different metallicities: $Z = 0.0002$, 0.004, and 0.04. A decrease in both the population size and maximum luminosity of HMXBs is observed as metallicity increases. The reduction in the number of HMXB systems at high metallicity occurs for several reasons, primarily affecting black holes, which are responsible for the highest luminosities. Stars with higher metallicity have a larger radius than those with lower metallicity, making them more prone to experiencing episodes of RLOF and/or CE (Linden et al., 2010). This leads to a decrease in the chances of surviving a dynamically unstable mass-transfer phase. Stronger stellar winds in these high-metallicity environments cause stars to retain less mass by the time they reach the supernova stage, leading to the formation of less massive compact objects. Additionally, these winds carry away angular momentum, leading to wider orbits on average. Consequently, the supernova kicks are more effective at disrupting binaries and reducing the population of HMXBs (Dray, 2006). Figure 2 presents the age distribution of HMXBs, again comparing systems across three different metallicities. The decrease in the number of systems older than 30 Myr in the high-metallicity case is

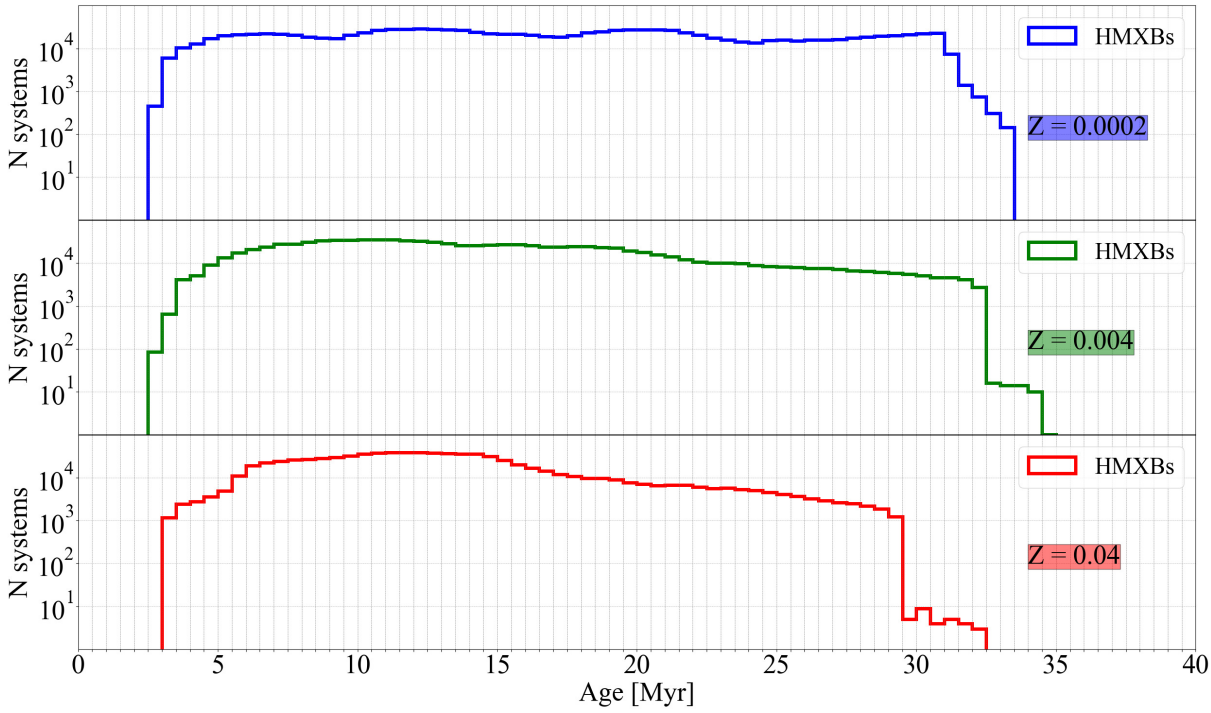

Figure 2: Age distribution of the HMXBs as a function of three different metallicities. As expected, no HMXBs form within the first 2 Myr, as this is insufficient time to produce the compact object from the more massive star in the system. After approximately 35 Myr, all systems have either become double compact objects, merged, or been disrupted.

mainly due to the significant mass loss these systems experience over their lifetimes, preventing the formation of persistent systems. This figure also shows that we do not expect to observe HMXB systems before approximately 2.5 Myr or beyond about 35 Myr; this will be important in Sect. 2.2.

2.2. IllustrisTNG50: MW/M31-like galaxies

Our methodology utilizes the IllustrisTNG50 (hereafter TNG50) simulation, which has the highest resolution in comparison to the other IllustrisTNG simulations. In particular, we use the selection of Milky Way- and Andromeda-like (MW/M31-like) galaxies from Pillepich et al. (2024). The TNG50 has a resolution for dark matter particles of $4.5 \times 10^5\,M_\odot$ and initial gas cells of $8.5 \times 10^4\,M_\odot$. The catalog from Pillepich et al. (2024) contains 198 MW/M31-like galaxies at $Z = 0$. From the 198 MW/M31-like galaxies, we select 151 galaxies with sufficient stellar particles (from 100 to approximately 8000 stellar particles per galaxy) to trace the star formation regions, such as the spiral arms. To assign HMXB events to each simulated galaxy, we first identify stellar particles that meet the following criteria: (1) they are within 65 Kpc from the galaxy center; (2) they have metallicities between 0.0002 and 0.04; (3) they have stellar ages of less than 40 Myr. The first criterion arises from the fact that galaxy cut-outs include all stellar particles within a cube of ± 400 cKpc from the galaxy's center, and we want to avoid populating

these particles. The second criterion comes from the fact that the HMXBs simulated are limited to $Z \leq 0.04$ due to the stellar tracks provided by PARSEC. The third criterion is because we do not expect any HMXBs after 40 Myr of the initial starburst. In the following section, we outline the process for populating the galaxy catalogs with HMXBs computed using SEVN.

2.3. Populating Galaxies: combining SEVN with TNG50

For each MW/M31-like galaxy, we estimate the number of HMXBs that correspond to each selected stellar particle (see Section 2.2) following a modified approach based on Artale et al. (2019a) (but see also, Mapelli et al. 2017 and Artale et al. 2019b):

$$N_{\rm HMXBs}(t_*, Z_*, m_*^{\rm TNG50}) = \frac{N_i^{\rm SEVN}(t_*, Z_*)}{m^{\rm SEVN}(Z_*)}\, m_*^{\rm TNG50} f_{\rm corr}\, f_{\rm bin}$$

where t_*, Z_* and $m_*^{\rm TNG50}$ are the age, metallicity, and mass of a stellar particle from TNG50, respectively, $N_i^{\rm SEVN}(t_*, Z_*)$ is the number of HMXBs in the age bin corresponding to the age t_* of the stellar particle with metallicity Z_*, $m^{\rm SEVN}(Z_*)$ is the total mass of the SEVN simulation closest to the metallicity of the stellar particle Z_*. The correction factor $f_{\rm corr} = 0.172$ accounts for the fact that we do not include the entire range of masses from the initial mass function in the simulation. We assume that the fraction of binaries is $f_{\rm bin} = 0.5$.

Some stellar particles have $N_{\rm HMXBs} < 1$, meaning they contain fewer than one HMXB. In this case, the value obtained for $N_{\rm HMXBs}$ is added to the value $N_{\rm HMXBs}$ of the subsequent stellar particle. This summation continues until the cumulative $N_{\rm HMXBs}$ value exceeds one. The HMXB is assigned to the first stellar particle where $N_{\rm HMXBs}$ exceeds one, after which the $N_{\rm HMXBs}$ value is reset.

Figure 3 shows the results of populating one galaxy from the sample; the panels display various properties of the stellar particles, which inherit the characteristics of HMXBs. In the top-left panel, we observe that the selection aligns with the regions of high star formation within the galaxy, where we expect HMXBs to be located. The bottom-left and top-right panels show the stellar age and X-ray luminosity, respectively. Although these do not display any clear patterns, further examination of the sample reveals that X-ray luminosities greater than $10^{37.5}\,{\rm erg\,s^{-1}}$ only originate from stellar particles with ages of less than 25 Myr and with the lowest metallicities. The bottom-right panel shows that particles with higher metallicities (red) tend to be more concentrated in the inner regions of the galaxy, while those with lower metallicities (blue) extend further towards the outskirts. This is consistent with expectations from galactic evolution and the way we populate stellar particles with HMXBs.

3. Results

The first comparison to perform is with the estimated ages since the first supernova event for 15 HMXBs associated with a birthplace (either an Open Cluster or a Spiral Arm) as reported by Fortin et al. (2022) shown in Fig. 4. These ages largely fall within the range of our simulations, with only two systems near the boundary: HD 259440 at 38^{+4}_{-4} Myr and SS 433 with an estimated age of less than 60 Myr. For SS 433, Fortin et al. (2022) identify two potential ages

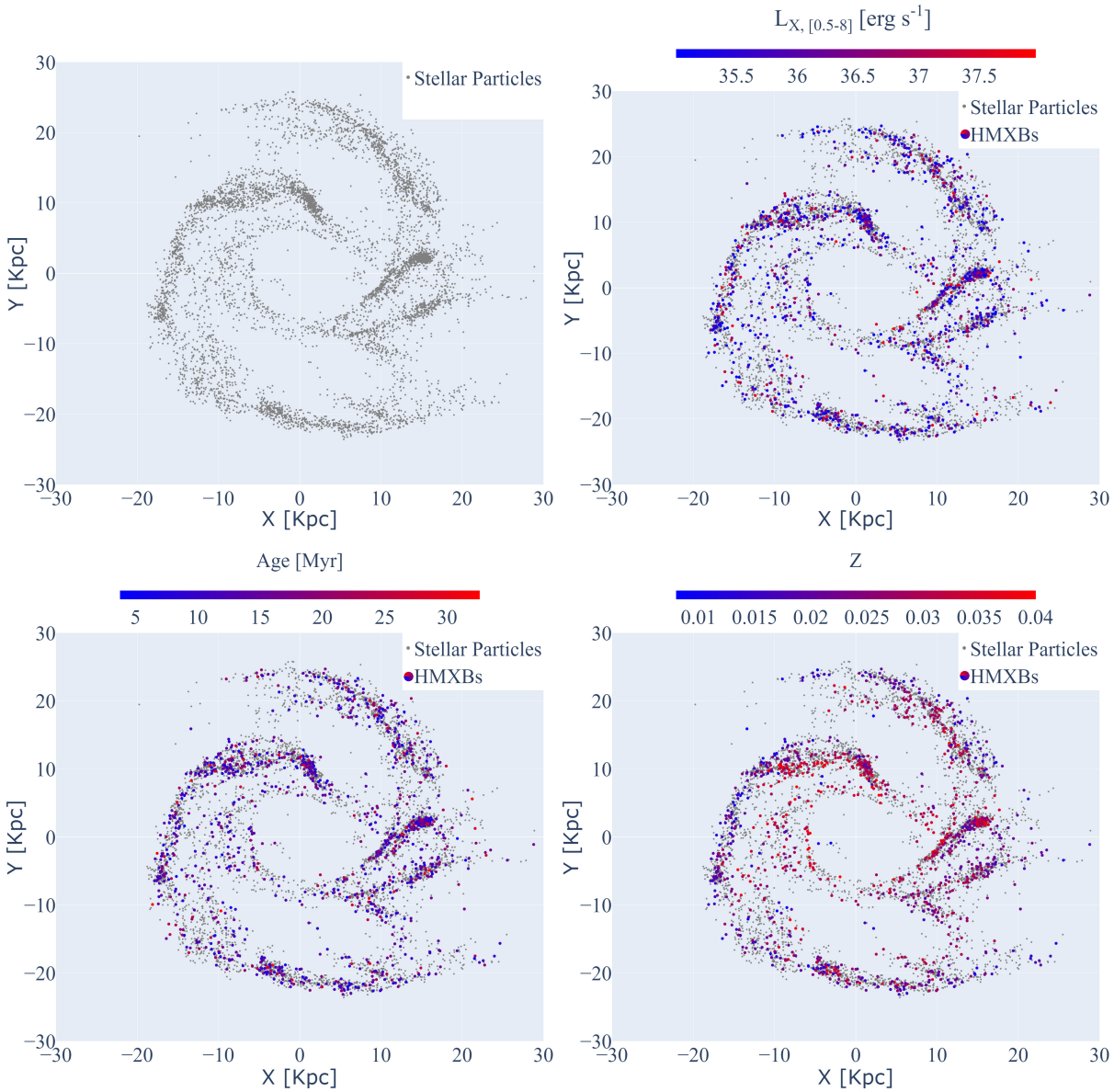

Figure 3: Face-on spatial distribution of the stellar particles of a sample galaxy. The colored points represent stellar particles populated with HMXBs, with each color indicating the specific property being analyzed. (*Top left*) Stellar particles in the galaxy that meet requirements (1), (2), and (3) of Sect. 2.2; these particles could potentially contain HMXBs. (*Top right*) X-ray luminosity of the stellar particles. (*Bottom left*) Ages of the stellar particles. (*Bottom right*) Metallicity of the stellar particles. The galaxy shown has SubfindID = 342447, SFR $= 15.392\,M_{\odot}\,\mathrm{yr}^{-1}$ and Stellar Mass $= 9.12 \times 10^{10}\,M_{\odot}$ at redshift $Z = 0$.

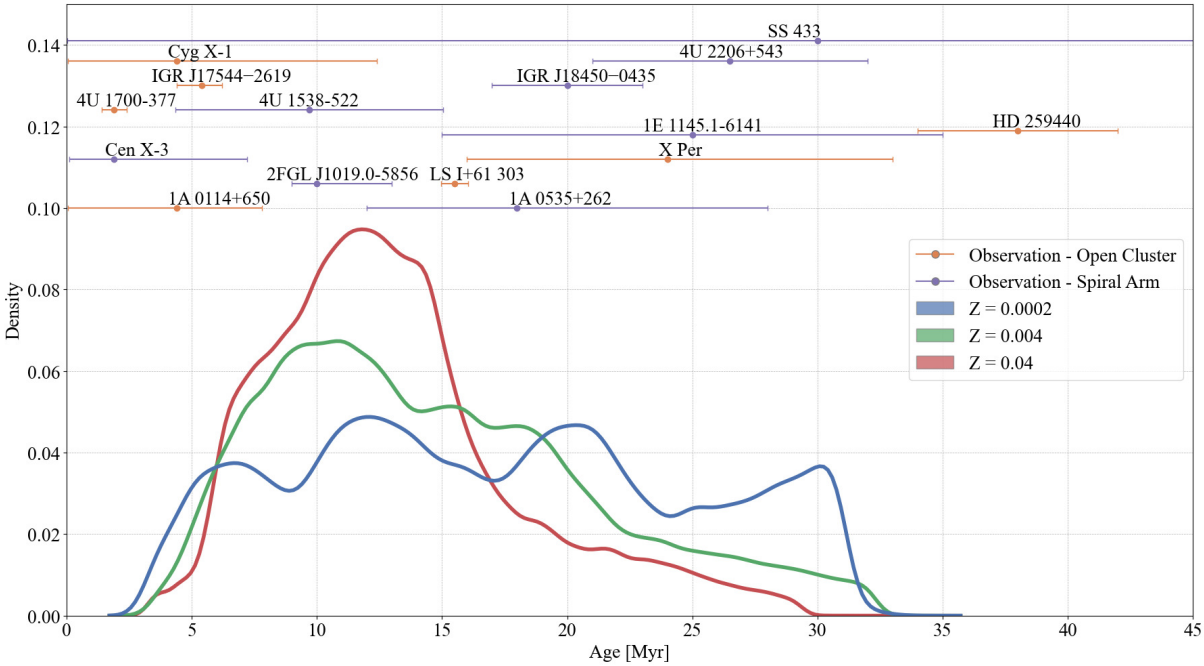

Figure 4: Density distribution of HMXB ages across three simulated metallicities and observational age estimates since the first supernova for 15 observed HMXBs. Ages are inferred based on the secondary mass following Eq. (3) from Fortin et al. (2022), with birthplaces determined using *Gaia* EDR3 data.

that could correspond to an encounter with the Sagittarius arm: 15 ± 1.5 Myr based on the mass estimation by Bowler (2018) or 58 ± 7 Myr based on the estimation by Picchi et al. (2020). Both estimates are consistent with our results.

Figure 5 (top panel) shows the relationship between the companion star mass and the compact object mass for the HMXBs population in simulated galaxies, in comparison with the catalog presented by Fortin et al. (2023). Our results indicate that the simulated HMXBs cover the masses around each of the 17 observed systems. One system with a companion star of mass $6.8 M_\odot$ is not accurately modeled, as it falls below our selection criterion of $\geq 8 M_\odot$ for the companion star. We note that our model successfully includes one of the most massive systems, Cygnus X-1, which has a black hole mass of $21.2 \pm 2.2 M_\odot$ and a companion star with a mass of $40.6^{+7.7}_{-7.1} M_\odot$ (Miller-Jones et al., 2021).

In Fig. 5 (bottom panel), we compare the eccentricity and orbital period of the simulated HMXBs with the data from the catalog of Fortin et al. (2023). In addition to the initial period distribution of the population that we choose, the luminosity cut ($> 10^{35}$ erg s^{-1}) also affects the sample of systems with long periods ($> 10^2$ days), as these systems will not be able to accrete sufficient material unless they have high eccentricities.

Considering this, our results show a good agreement with the observations for HMXBs with BHs and NSs.

We next compute the XLF from HMXBs for each simulated MW/M31-like galaxy and

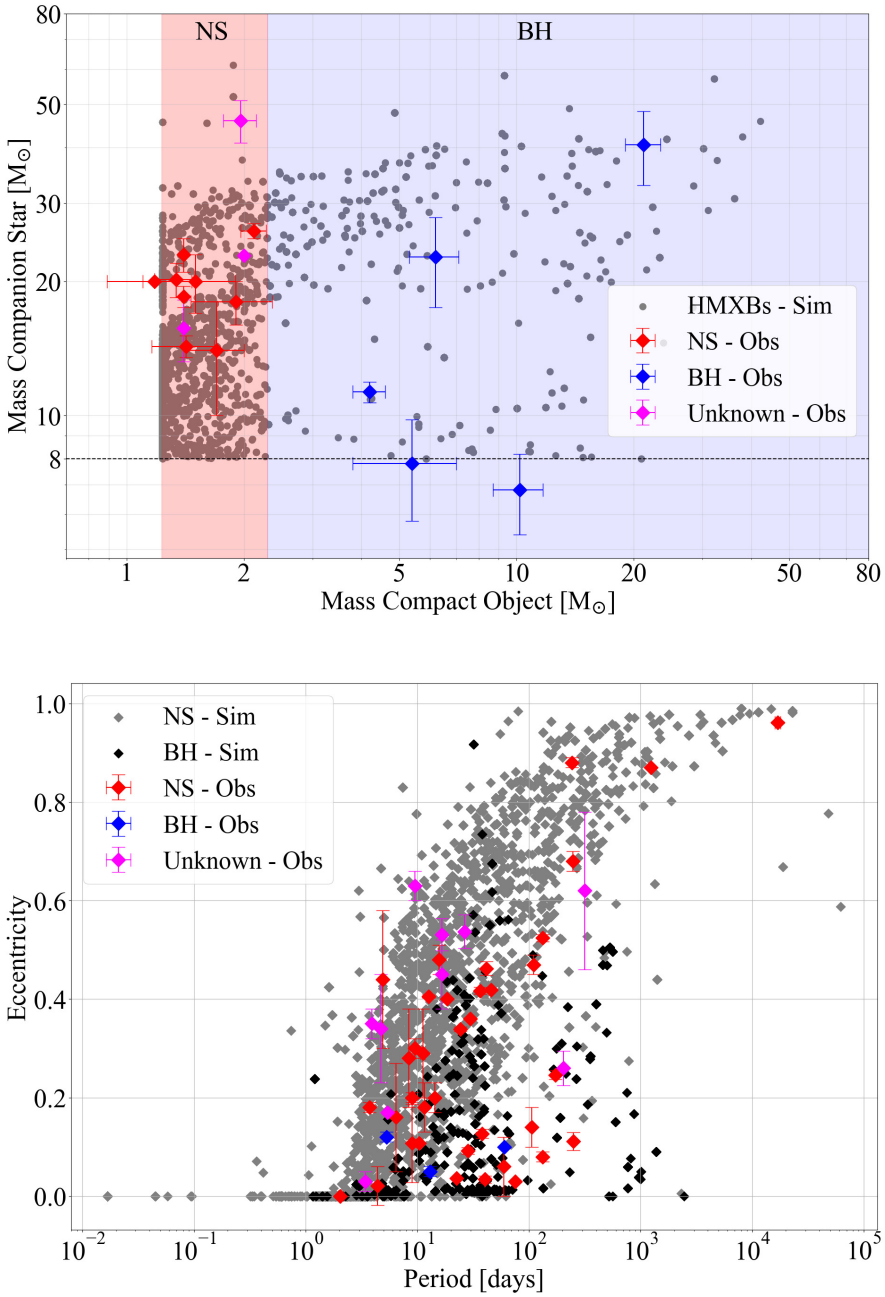

Figure 5: (*Top*) The companion star mass and compact object mass distribution of the HMXB population. Grey points represent the population of HMXBs in the simulated galaxies. Red and blue points indicate the mass measurements from the catalog of Fortin et al. (2023) for NS and BH, respectively. Red/blue shaded regions correspond to the NS/BH regions adopted in SEVN. The horizontal black line represents our cut in the companion stars of the HMXBs. (*Bottom*) Orbital parameters of the simulated HMXB population. compared the catalog of Fortin et al. (2023). In the panels, points represent our simulation (BH: black; NS: grey) and observations (BH: blue; NS: red), whereas magenta symbols indicate compact objects with an unknown remnant type.

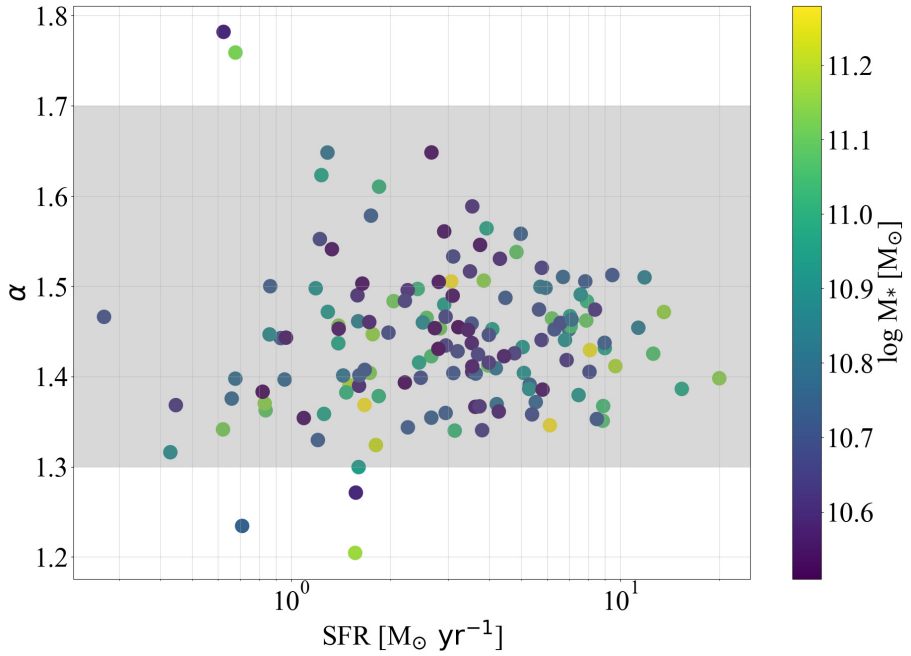

Figure 6: Slopes of the power law fit to the XLF for the populated galaxies. The grey band indicates the range of the slope values expected ($1.3 \leq \alpha \leq 1.7$) for the MW according to Fornasini et al. (2024). The color code represents the stellar mass of the MW/M31-like simulated galaxies.

fit them with a power-law. In Fig. 6 we compare the slopes (α) obtained from the XLF fits with the values from observations. Our findings indicate that the slopes obtained from our simulations generally fall within the observed range of $\alpha \approx 1.3$–1.7 from Fornasini et al. (2024), demonstrating consistency with the observational data.

4. Summary

In this study we investigate the population of HMXBs in simulated MW/M31-like galaxies using the IllustrisTNG50 hydrodynamical simulation (Pillepich et al., 2024; Nelson et al., 2019) in combination with the SEVN population synthesis code (Iorio et al., 2023; Spera et al., 2015) and PARSEC stellar tracks (Bressan et al., 2012; Nguyen et al., 2022). The methodology involved the selection of stellar particles from galaxies based on spatial location, metallicity, and age, and populating these particles with HMXBs. Our model represents a modified approach based on Mapelli et al. (2017); Artale et al. (2019a,b). The results show a clear decrease in both the population and luminosity of HMXBs as the metallicity increases. This behavior is consistent with previous findings (Dray, 2006; Linden et al., 2010). Our simulations properly reproduce the X-ray luminosity function slope, orbital parameters, and masses of HMXBs, consistent with the observations of the current Milky Way catalog by Fortin et al. (2023). We will further examine how changing key parameters in SEVN, such as common envelope and accretion efficiency, will impact the population properties of simulated HMXBs. This extended analysis will be detailed in a subsequent article.

Acknowledgments

We thank the referee for their useful comments. The authors thank Michela Mapelli for her comments. This work was funded by the National Agency for Research and Development (ANID) / Scholarship Program / DOCTORADO NACIONAL / 2021 – 21222248. MCA and FV acknowledge support from FONDECYT Iniciación 11240540. MCA acknowledges support from ANID BASAL project FB210003. GJE acknowledges financial support from the European Research Council for the ERC Consolidator grant DEMOBLACK, under contract no. 770017. GI acknowledges financial support under the National Recovery and Resilience Plan (NRRP), Mission 4, Component 2, Investment 1.4 – Call for tender No. 3138 of 18/12/2021 of Italian Ministry of University and Research funded by the European Union – NextGenerationEU.

Further Information

Authors' ORCID identifiers

0000-0001-9352-2286 (Felipe VIVANCO CÁDIZ)
0000-0003-0570-785X (M. Celeste ARTALE)
0000-0001-9487-7740 (Nicola MASETTI)
0000-0003-0293-503X (Giuliano IORIO)
0000-0002-4007-7585 (Gastón J. ESCOBAR)

Author contributions

Felipe Vivanco Cádiz: Writing – Original Draft, Writing – Review & Editing, Methodology, Software, Formal analysis, Investigation, Visualization.

Maria Celeste Artale: Writing – Original Draft, Writing – Review & Editing, Supervision, Resources, Validation, Methodology, Conceptualization.

Nicola Masetti: Writing – Review & Editing, Investigation, Resources, Supervision.

Gastón J. Escobar: Writing – Review & Editing, Software, Methodology.

Giuliano Iorio: Writing – Review & Editing, Software, Methodology.

Conflicts of interest

The authors declare that there is no conflict of interest.

References

Anastasopoulou, K., Zezas, A., Steiner, J. F., and Reig, P. (2022) Average bolometric corrections and optical to X-ray flux measurements as a function of accretion rate for X-ray binaries. *MNRAS*, **513**(1), 1400–1413. https://doi.org/10.1093/mnras/stac940.

Artale, M. C., Giacobbo, N., Mapelli, M., and Esposito, P. (2019a) The high mass X-ray binaries in star-forming galaxies. *Proceedings of the International Astronomical Union*, **14**(S346), 332–336. https://doi.org/10.1017/S1743921318007627.

Artale, M. C., Mapelli, M., Giacobbo, N., Sabha, N. B., Spera, M., Santoliquido, F., and Bressan, A. (2019b) Host galaxies of merging compact objects: mass, star formation rate, metallicity, and colours. *MNRAS*, **487**(2), 1675–1688. https://doi.org/10.1093/mnras/stz1382.

Bowler, M. G. (2018) SS 433: Two robust determinations fix the mass ratio. *A&A*, **619**, L4. https://doi.org/10.1051/0004-6361/201834121.

Bressan, A., Marigo, P., Girardi, L., Salasnich, B., Dal Cero, C., Rubele, S., and Nanni, A. (2012) PARSEC: stellar tracks and isochrones with the PAdova and TRieste Stellar Evolution Code. *MNRAS*, **427**(1), 127–145. https://doi.org/10.1111/j.1365-2966.2012.21948.x.

Campana, S., Stella, L., Mereghetti, S., and de Martino, D. (2018) A universal relation for the propeller mechanisms in magnetic rotating stars at different scales. *A&A*, **610**, A46. https://doi.org/10.1051/0004-6361/201730769.

Douna, V. M., Pellizza, L. J., Mirabel, I. F., and Pedrosa, S. E. (2015) Metallicity dependence of high-mass X-ray binary populations. *A&A*, **579**, A44. https://doi.org/10.1051/0004-6361/201525617.

Dray, L. M. (2006) On the metallicity dependence of high-mass X-ray binaries. *MNRAS*, **370**(4), 2079–2090. https://doi.org/10.1111/j.1365-2966.2006.10635.x.

Fishbach, M. and Kalogera, V. (2022) Apples and oranges: Comparing black holes in X-ray binaries and gravitational-wave sources. *ApJL*, **929**(2), L26. https://doi.org/10.3847/2041-8213/ac64a5.

Fornasini, F., Antoniou, V., and Dubus, G. (2024) High-mass X-ray binaries. In *Handbook of X-ray and Gamma-ray Astrophysics*, edited by Bambi, C. and Santangelo, A., pages 3719–3773. Springer Nature, Singapore. https://doi.org/10.1007/978-981-19-6960-7_95.

Fortin, F., García, F., and Chaty, S. (2022) Finding the birthplace of HMXBs in the Galaxy using *Gaia* EDR3: Kinematical age determination through orbit integration. *A&A*, **665**, A69. https://doi.org/10.1051/0004-6361/202244048.

Fortin, F., García, F., Simaz Bunzel, A., and Chaty, S. (2023) A catalogue of high-mass X-ray binaries in the Galaxy: from the INTEGRAL to the *Gaia* era. *A&A*, **671**, A149. https://doi.org/10.1051/0004-6361/202245236.

Fragos, T., Lehmer, B., Tremmel, M., Tzanavaris, P., Basu-Zych, A., Belczynski, K., Hornschemeier, A., Jenkins, L., Kalogera, V., Ptak, A., and Zezas, A. (2013) X-ray binary evolution across cosmic time. *ApJ*, **764**(1), 41. https://doi.org/10.1088/0004-637X/764/1/41.

Fryer, C. L., Belczynski, K., Wiktorowicz, G., Dominik, M., Kalogera, V., and Holz, D. E. (2012) Compact remnant mass function: Dependence on the explosion mechanism and metallicity. *ApJ*, **749**(1), 91. https://doi.org/10.1088/0004-637X/749/1/91.

Grimm, H.-J., Gilfanov, M., and Sunyaev, R. (2003) High-mass X-ray binaries as a star formation rate indicator in distant galaxies. *MNRAS*, **339**(3), 793–809. https://doi.org/10.1046/j.1365-8711.2003.06224.x.

Hurley, J. R., Tout, C. A., and Pols, O. R. (2002) Evolution of binary stars and the effect of tides on binary populations. *MNRAS*, **329**(4), 897–928. https://doi.org/10.1046/j.1365-8711.2002.05038.x.

Iorio, G., Mapelli, M., Costa, G., Spera, M., Escobar, G. J., Sgalletta, C., Trani, A. A., Korb, E., Santoliquido, F., Dall'Amico, M., Gaspari, N., and Bressan, A. (2023) Compact object mergers: exploring uncertainties from stellar and binary evolution with SEVN. *MNRAS*, **524**(1), 426–470. https://doi.org/10.1093/mnras/stad1630.

Kroupa, P. (2001) On the variation of the initial mass function. *MNRAS*, **322**(2), 231–246. https://doi.org/10.1046/j.1365-8711.2001.04022.x.

Lehmer, B. D., Eufrasio, R. T., Basu-Zych, A., Doore, K., Fragos, T., Garofali, K., Kovlakas, K., Williams, B. F., Zezas, A., and Santana-Silva, L. (2021) The metallicity dependence of the high-mass X-ray binary luminosity function. *ApJ*, **907**(1), 17. https://doi.org/10.3847/1538-4357/abcec1.

Linden, T., Kalogera, V., Sepinsky, J. F., Prestwich, A., Zezas, A., and Gallagher, J. S. (2010) The effect of starburst metallicity on bright X-ray binary formation pathways. *ApJ*, **725**(2), 1984–1994. https://doi.org/10.1088/0004-637X/725/2/1984.

Mapelli, M., Colpi, M., and Zampieri, L. (2009) Low metallicity and ultra-luminous X-ray sources in the Cartwheel galaxy. *MNRAS*, **395**(1), L71–L75. https://doi.org/10.1111/j.1745-3933.2009.00645.x.

Mapelli, M., Giacobbo, N., Ripamonti, E., and Spera, M. (2017) The cosmic merger rate of stellar black hole binaries from the Illustris simulation. *MNRAS*, **472**(2), 2422–2435. https://doi.org/10.1093/mnras/stx2123.

Miller-Jones, J. C. A., Bahramian, A., Orosz, J. A., Mandel, I., Gou, L., Maccarone, T. J., Neijssel, C. J., Zhao, X., Ziółkowski, J., Reid, M. J., Uttley, P., Zheng, X., Byun, D.-Y., Dodson, R., Grinberg, V., Jung, T., Kim, J.-S., Marcote, B., Markoff, S., Rioja, M. J., Rushton, A. P., Russell, D. M., Sivakoff, G. R., Tetarenko, A. J., Tudose, V., and Wilms, J. (2021) Cygnus X-1 contains a 21-solar mass black hole—implications for massive star winds. *Sci*, **371**, 1046–1049. https://doi.org/10.1126/science.abb3363.

Mineo, S., Gilfanov, M., and Sunyaev, R. (2012) X-ray emission from star-forming galaxies – I. High-mass X-ray binaries. *MNRAS*, **419**(3), 2095–2115. https://doi.org/10.1111/j.1365-2966.2011.19862.x.

Misra, D., Kovlakas, K., Fragos, T., Lazzarini, M., Bavera, S. S., Lehmer, B. D., Zezas, A., Zapartas, E., Xing, Z., Andrews, J. J., Dotter, A., Rocha, K. A., Srivastava, Ph. M., and Sun, M. (2023) X-ray luminosity function of high-mass X-ray binaries: Studying the signatures of different physical processes using detailed binary evolution calculations. *A&A*, **672**, A99. https://doi.org/10.1051/0004-6361/202244929.

Nathanail, A., Most, E. R., and Rezzolla, L. (2021) GW170817 and GW190814: Tension on the maximum mass. *ApJL*, **908**(2), L28. https://doi.org/10.3847/2041-8213/abdfc6.

Nelson, D., Pillepich, A., Springel, V., Pakmor, R., Weinberger, R., Genel, S., Torrey, P., Vogelsberger, M., Marinacci, F., and Hernquist, L. (2019) First results from the TNG50 simulation: galactic outflows driven by supernovae and black hole feedback. *MNRAS*, **490**(3), 3234–3261. https://doi.org/10.1093/mnras/stz2306.

Nguyen, C. T., Costa, G., Girardi, L., Volpato, G., Bressan, A., Chen, Y., Marigo, P., Fu, X., and Goudfrooij, P. (2022) PARSEC V2.0: Stellar tracks and isochrones of low- and intermediate-mass stars with rotation. *A&A*, **665**, A126. https://doi.org/10.1051/0004-6361/202244166.

Picchi, P., Shore, S. N., Harvey, E. J., and Berdyugin, A. (2020) An optical spectroscopic and polarimetric study of the microquasar binary system SS 433. *A&A*, **640**, A96. https://doi.org/10.1051/0004-6361/202037960.

Pillepich, A., Sotillo-Ramos, D., Ramesh, R., Nelson, D., Engler, C., Rodriguez-Gomez, V., Fournier, M., Donnari, M., Springel, V., and Hernquist, L. (2024) Milky Way and Andromeda analogues from the TNG50 simulation. *MNRAS*, **535**(2), 1721–1762. https://doi.org/10.1093/mnras/stae2165.

Podsiadlowski, Ph., Rappaport, S., and Han, Z. (2003) On the formation and evolution of black hole binaries. *MNRAS*, **341**(2), 385–404. https://doi.org/10.1046/j.1365-8711.2003.06464.x.

Sana, H., de Mink, S. E., de Koter, A., Langer, N., Evans, C. J., Gieles, M., Gosset, E., Izzard, R. G., Le Bouquin, J.-B., and Schneider, F. R. N. (2012) Binary interaction dominates the evolution of massive stars. *Sci*, **337**, 444–446. https://doi.org/10.1126/science.1223344.

Sgalletta, C., Iorio, G., Mapelli, M., Artale, M. C., Boco, L., Chattopadhyay, D., Lapi, A., Possenti, A., Rinaldi, S., and Spera, M. (2023) Binary neutron star populations in the Milky Way. *MNRAS*, **526**(2), 2210–2229. https://doi.org/10.1093/mnras/stad2768.

Spera, M., Mapelli, M., and Bressan, A. (2015) The mass spectrum of compact remnants from the PARSEC stellar evolution tracks. *MNRAS*, **451**(4), 4086–4103. https://doi.org/10.1093/mnras/stv1161.

van den Heuvel, E. P. J. (2019) High-mass X-ray binaries: progenitors of double compact objects. *Proceedings of the International Astronomical Union*, **14**(S346), 1–13. https://doi.org/10.1017/S1743921319001315.